Graphene Phosphonic Acid as an Efficient Flame Retardant

Min-Jung Kim,[†,§] In-Yup Jeon,[†,§] Jeong-Min Seo,[†] Liming Dai,[‡,*] and Jong-Beom Baek[†,*]

[†]School of Energy and Chemical Engineering/Low-Dimensional Carbon Materials Center, Ulsan National Institute of Science and Technology (UNIST), 100 Banyeon, Ulsan 689-897, South Korea and [‡]Department of Macromolecular Science and Engineering, Case Western Reserve University, 10900 Euclid Avenue, Cleveland, Ohio 44106, United States. [§]These authors contributed equally.

ABSTRACT We report the preparation of graphene phosphonic acid (GPA) *via* a simple and versatile method and its use as an efficient flame retardant. In order to covalently attach phosphorus to the edges of graphene nanoplatelets, graphite was ball-milled with red phosphorus. The cleavage of graphitic C—C bonds during mechanochemical ball-milling generates reactive carbon species, which react with phosphorus in a sealed ball-mill crusher to form graphene phosphorus. Subsequent opening of the crusher in air moisture leads to violent oxidation of graphene phosphorus into GPA (highest oxidation state). The GPA is readily dispersible in many polar solvents, including neutral water, allowing for solution (spray) coating for high-performance, nontoxic flame-retardant applications.

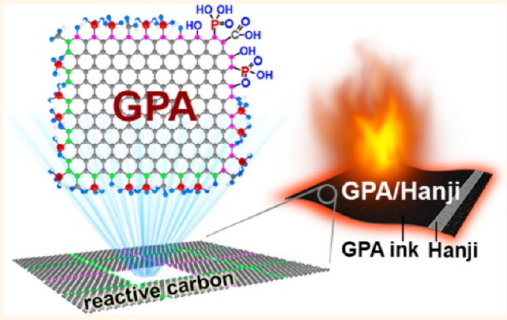

KEYWORDS: graphene phosphonic acid · flame retardation · ball-milling · edge functionalization

Phosphorus (P) is an important constituent element for many commercial products, including fertilizers, detergents, pesticides, flame retardants, and even matches.[1] It is also essential for life, as a major component of ATP, DNA, and RNA in the form of phosphates,[2] as well as cell membranes in the form of phospholipids.[3] Phosphorus has a few different forms (which have varying colors) with different physical properties and chemical reactivity. Elemental phosphorus mainly exists as white (yellow) phosphorus. White phosphorus has a P_4 tetrahedral structure, which can be transformed into red phosphorus by heat and/or radiation.[4] Unlike white phosphorus that is dangerously reactive and toxic to handle in practice, red phosphorus has a stable amorphous polymeric structure.

On the other hand, graphite has a two-dimensional (2D) layered structure and is the most thermodynamically stable form among all of the carbon allotropes.[5] Due to this stability, it is often difficult to incorporate heteroatoms into graphitic carbon networks *via* either direct chemical modification or chemical vapor deposition (CVD).[6] Although many recent reports[7] have demonstrated the possibility of producing heteroatom-doped graphene nanoplatelets (GnPs) from graphene oxides (GOs),[8] the mechanistic pathway and structure of the heteroatom-doped GOs cannot be well-defined and controlled.[9] To overcome this limitation by incorporating heteroatom(s) directly at the edges of graphitic carbon networks, we devised an efficient mechanochemical (ball-milling) method for the direct formation of C—Z (Z = COOH),[10] C—Y (Y = H, NH_2, SO_3H),[10,11] C—X (X = Cl, Br, I),[12] C—N (N = aromatic pyrazole N and pyridazine N),[13] C—S bonds,[14] as well as a pericyclic reaction.[15] Ball-milling graphite in the presence of various gas (H_2, NH_3, Cl_2, N_2, CO_2), liquid (SO_3, Br_2), and solid (I_2, S_8) reactants in a sealed crusher has been exploited to produce edge-selectively functionalized graphene nanoplatelets (EFGnPs) for energy conversion and storage applications.[10−13] Hence, the mechanochemical method to produce EFGnPs becomes a general procedure, which has advantages over the process for GOs in terms of manufacturing simplicity, scalability, and edge-selectivity.[16]

By using the newly developed ball-milling method for the synthesis of GnPs,[10] we, in the present study, attempted direct C—P bond formation at the broken edges of GnPs by dry ball-milling graphite with red

* Address correspondence to jbbaek@unist.ac.kr, liming.dai@case.edu.

Received for review December 29, 2013 and accepted February 27, 2014.

Published online February 27, 2014
10.1021/nn4066395

phosphorus (much safer than white phosphorus for handling) for 48 h. Upon exposure to air moisture, the resultant GnPs edge-functionalized with phosphorus spontaneously oxidized into graphene phosphonic acid (GPA). The loading amount of phosphorus could reach up to 23.9 wt % — the highest value among all reported heteroatom-doped GnPs (*e.g.*, ~14 wt % nitrogen),[13] though loading level is controllable by adjusting the ball-milling time (*vide infra*). Owing to the polar nature of phosphonic acid, GPA is readily dispersible in most polar solvents including neutral water (Supporting Information Figure S1a,b) even without physical agitation (see video in Supporting Information). Aqueous GPA solutions displayed zeta-potential values of −40.4, −46.5, and −33.3 mV at concentrations of 0.40, 0.50, and 0.60 mg/mL (Figure S1c and Table S1), respectively. It is well-known that an absolute value of the zeta-potential over 30 mV is sufficient to ensure good dispersion stability *via* charge repulsion.[17] GPA in water (0.5 mg/mL) is the highest achievable concentration among values for stable GnP dispersions.[18] Since phosphorus compounds are well-known for flame retardation,[19−21] an aqueous solution of GPA was coated onto a piece of paper (Hanji from Paper Mulberry) to test the flame retardation properties. The results demonstrate promise for GPA to be used for fire protection.

Figure 1a shows that ball-milling graphite generates active carbon species (mostly carboradicals),[22] which react with phosphorus. The resultant graphene phosphorus was subsequently oxidized to GPA upon exposure to air moisture as phosphorus is highly susceptible to maximum oxidation by oxygen (GnP−PO_3H_2, in this work).[23] Comparing Figure 1b with Figure 1c clearly shows significant grain size reduction from the starting graphite (100 mesh, <150 μm, Figure 1b) to GPA (<4 μm, Figure 1c) due to the mechanochemical cracking associated with the ball-milling process. The total available active carbons at the broken edges could be estimated from an average grain size reduction by eq 1.[13]

$$8a\sum_{k=1}^{n}\left(\frac{1}{2}\right)^{k}\cdot 4^{k-1} = 2a\sum_{k=1}^{n}2^{k} \qquad (1)$$

where a is the initial average number of carbon atoms at the edges of the starting graphite and k is the number of cross-cutting. As a simple model (Figure S2), a square-shaped graphene with 100 carbons (a = 100) at an edge and with three cross-cuts (k = 3) can generate 2800 active carbons, that is, 2800/10 000 × 100 = 28% active carbons, though they may not completely react with phosphorus. On the basis of elemental analysis (EA, Table S2) and EDX element mapping (Figure S3), phosphorus content in GPA was as high as 23.9 wt % and 21.2 at %, respectively, after thoroughly washing off the unreacted phosphorus residues during the workup process (see the detailed workup procedure in the Methods section).

The results from SEM (Figure 1b,c) and EA (Table S2) imply that multiple cross-cuttings have indeed occurred, which led to an oxygen content of 35.9 wt %, equivalent to an O/P atomic ratio of 2.9, which is close to the 3 for $-PO_3H_2$. Thus, the oxidation of edge-phosphorus-attached GnPs (GnP−P) into graphene phosphonic acid (GnP−PO_3H_2, GPA) is a weight-gaining (from 5.00 g starting graphite to 10.17 g GPA) spontaneous process.[23] Upon dispersion of GPA in a solvent, further solvent-assisted exfoliation could be expected.

In order to demonstrate the control over the phosphorus content and grain size of GPA by adjusting the ball-milling time, graphite was ball-milled in the presence of red phosphorus for 12 h. The sample displayed phosphorus content of 14.5 wt % (EA, Table S2) and a grain size of 300−500 nm (SEM, Figure S5), suggesting that the element content and grain size are controllable by mechanochemical ball-milling time.

The Raman spectrum of the starting graphite showed the G and 2D bands at 1584 and 2721 cm^{-1}, respectively (Figure 2a), with undetectable edge distortion and structural defects, and hence the D to G band intensity ratio (I_D/I_G) approached zero. On the other hand, powder GPA exhibited a broad and strong D band over 1340 cm^{-1}. The I_D/I_G ratio is 0.96 (Figure 2a), implying significant edge distortion resulting from the grain size reduction by the mechanochemical cracking of graphitic C−C bonds (see Figure 1c) and the subsequent edge functionalization with phosphonic acid groups (see Figure 1a).

The X-ray diffraction (XRD) pattern for the starting graphite showed a strong [002] peak at 26.5° corresponding to a layer-to-layer d-spacing of 0.34 nm (Figure 2b).[24] By contrast, the XRD pattern for GPA exhibited only a very weak [002] peak centered at 22.5° (Figure 2b). These results indicate that significant delamination of the highly crystalline graphite into GPA has occurred even in the solid state during the ball-milling and subsequent workup processes.

The Fourier transform infrared (FT-IR) spectrum of GPA shows strong aromatic C−P, P═O, P−O, and P−OH stretching peaks at 1147, 1176, 1011, and 938 cm^{-1}, respectively (Figure 2c; the detailed peak assignments are presented in Figure S6). The strong peaks at around 3400 and 1630 cm^{-1} indicate the hygroscopic nature of GPA, though crystal water associated with the KBr used for the preparation of the IR specimen cannot be ruled out. The solid-state ^{31}P magic-angle spinning (MAS) NMR spectrum of GPA shows broad peaks at around 0 ppm, which are attributable to the C−P(═O)(−OH)$_2$ of phosphonic acid (Figure S7, with the detailed peak assignments).

XPS spectroscopic measurements further revealed the presence of phosphorus in GPA. Compared with the starting graphite, showing prominent C 1s and weak O 1s peaks at 284.3 and 532 eV, respectively (Figure 2d),[25] GPA showed the characteristic P 2s and

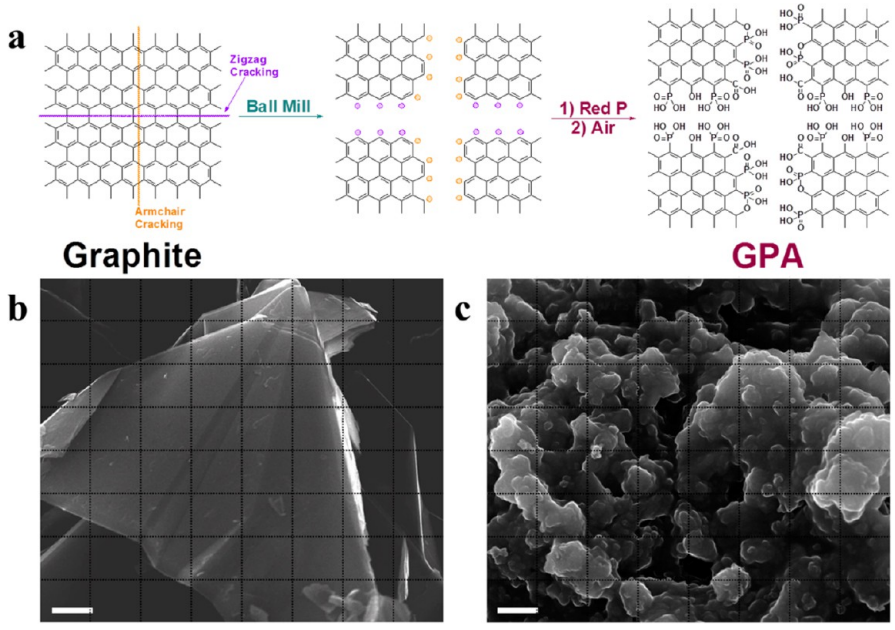

Figure 1. (a) Schematic representation of mechanochemical cracking of a graphite flake in a ball-mill crusher containing stainless steel balls (diameter 5 mm) in the presence of red phosphorus and subsequent exposure to air moisture to produce GPA (see also Figure S4). The structure of graphite is simplified for clarity. SEM images: (b) starting graphite flake (100 mesh, <150 μm); (c) GPA (<4 μm). Scale bars are 4 μm. Grid lines are presented to explain availability of active carbons after cracking (see also Figure S2).

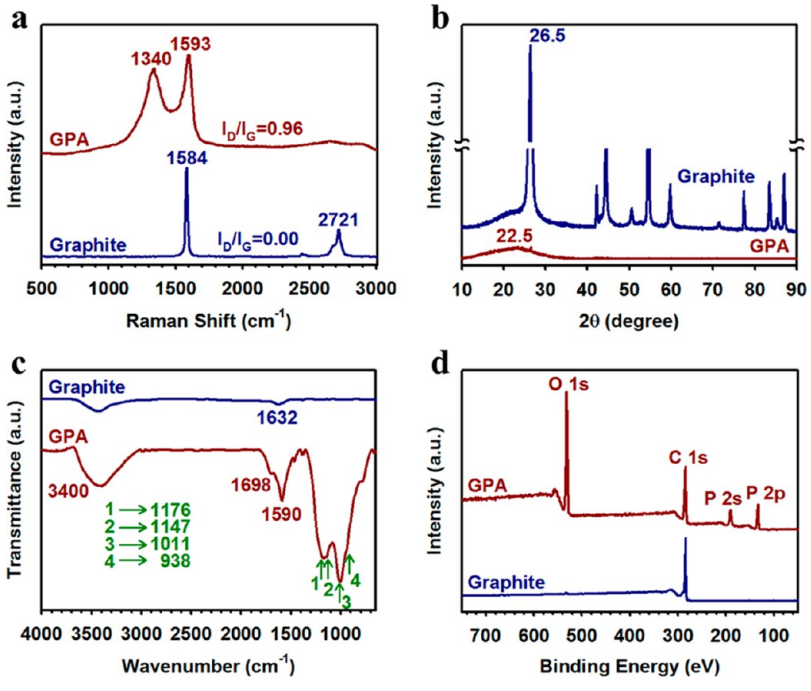

Figure 2. (a) Raman spectra obtained from a He−Ne laser (532 nm) as the excitation source. (b) XRD diffraction patterns. (c) FT-IR spectra (KBr pellets), clearly showing C−P stretching peak at 1147 cm^{-1} (detailed assignments for other peaks are presented in Figure S6). (d) XPS survey spectra (high-resolution XPS spectra are presented in Figure S8).

P 2p peaks at 191 and 135 eV, respectively, in addition to strong C 1s and O 1s peaks. High-resolution XPS spectra with curve fittings for the C 1s (Figure S8a), O 1s (Figure S8b), P 2s (Figure S8c), and P 2p (Figure S8d) peaks showed that the aromatic C−P, P−O, and P═O are the dominant P components in GPA. Overall, the XPS measurements agreed well with the FT-IR (see Figures 2c and S6) and ^{31}P NMR results (see Figure S7), supporting the structure of GPA proposed in Figure 1a.

Thermogravimetric analysis (TGA) of the GPA in air showed stepwise weight losses at around 153 and 581 °C, while the pristine graphite was stable up to 800 °C (Figure S9). The thermally induced loss of bound water is responsible for the early weight loss at 153 °C,

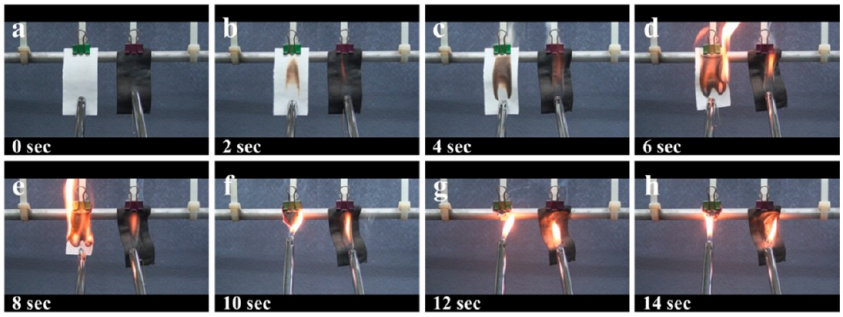

Figure 3. Snapshots of flame treatments of Hanji (left) and GPA/Hanji (right) with respect to time in second: (a–h) 0–14 s. The images were captured from the video in the Supporting Information.

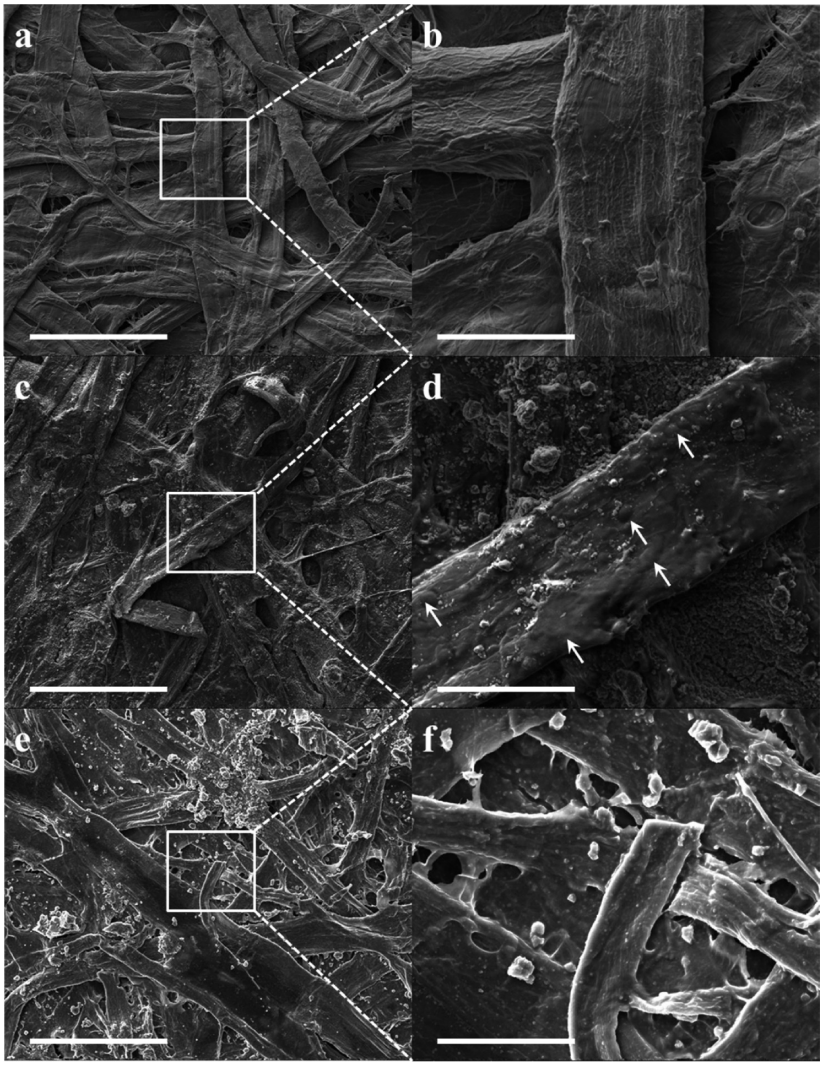

Figure 4. SEM images at different magnifications: (a,b) Hanji; (c,d) GPA/Hanji; (e,f) flame-treated GPA/Hanji. Scale bars are 100 μm (a,c,e) and 20 μm (b,d,f).

implying the hygroscopic nature of phosphonic acid, as also indicated by the FT-IR spectrum (Figure S6). The major weight loss at 581 °C is attributable to thermal condensation of phosphonic acid (Figure S10) and the subsequent decomposition of the graphitic framework in air. The TGA thermogram obtained under a nitrogen atmosphere displayed three step weight losses at around 151, 496, and 866 °C. The polar hygroscopic nature of phosphonic acid at the edges of GPA was once again confirmed by the initial weight loss related to bound moisture. The second weight loss was attributed to thermal condensation of phosphonic acid into pyrophosphonic acid and metaphosphonic acid, releasing water as a byproduct.[26] The weight loss at

866 °C could be due to the pyrolysis of graphitic carbon and phosphorus. The flame retardation of GPA should be attributable to the above-mentioned physical and chemical processes.[14]

Having confirmed the structure of GPA and its dispersibility in neutral water, we prepared a high-concentration (0.2 mg/mL) GPA ink in water for further investigation of flame retardant applications. For the preparation of flame retardation sample, pieces (3.5 × 7.5 cm) of Hanji (left in Figure S11a, fibrous paper from Paper Mulberry) was not coated with GPA ink, while the other piece was coated with GPA ink and dried under vacuum at 50 °C overnight (right in Figure S11a). The average loading amount of GPA to Hanji was 13.6 ± 2.58 wt % (Table S3). The Hanji and GPA-coated Hanji (GPA/Hanji) were torched in air with a propane gas flame at the same time (Figure 3 and video in Supporting Information). The pristine Hanji completely burned off in 10 s, leaving trace amounts of white ash (left in Figure S11b). On the other hand, the GPA/Hanji emitted white smoke at the beginning without catching fire and maintained the initial shape with little shrinkage. For the comparison, graphene oxide (GO)/Hanji specimen was also prepared as followed by the same procedure for the preparation of GPA/Hanji (see details in Methods section). As shown in Figure S12a, GO could not be uniformly coated on Hanji and the GO/Hanji caught flame (Figure S12b). On the other hand, the GPA/Hanji just emitted white smoke without catching fire, suggesting that GPA had obvious advantages over GO as a flame retardant.

On the basis of TGA (see Figure S9) and the proposed retardation mechanism (Figure S10), the initial smoke came from the steam produced by the physically bound moisture, along with the byproducts from the phosphonic acid condensation (Figure S13a) and thermal decomposition of GPA. Pyrolysis gas chromatography–mass spectrometry (Py/GC/MS) was used to identify the fumes in the temperature range of 200–600 °C (Figure S13b). Minor species in the temperature range of 290–360 °C could be assignable to phosphorus derivatives. Graphitic residue was a major component above 500 °C. Therefore, physical causes of retardation are related to the cooling of the burning surface by endothermic reactions and vaporization. Chemical retardation is related to the thermal condensation of phosphonic acid (Figure S12a) into char formation on the surface of solid fuel (Hanji).

The surface of the Hanji before flame treatment shows a fibrous sheet texture (Figure 4a,b). The GPA/Hanji before flame treatment displays a coarse morphology due to the GPA deposition on the surface of the Hanji (arrows, Figure 4c,d). After flame treatment, the GPA/Hanji maintains a fibrous morphology, supporting protective layer formation on the surface of the Hanji (Figure 4e,f). In comparison between the cross-sectional SEM images of the Hanji (Figure S11c) before torching and the GPA/Hanji (Figure S11d) after torching, the torched GPA/Hanji still exhibits fibrous textures. Hence, the GPA played key roles in flame retardation (Figure S13a).

CONCLUSION

We have developed a simple and eco-friendly ball-milling process to efficiently exfoliate pristine graphite directly into graphene phosphonic acid. A plausible reaction mechanism for the direct introduction of phosphorus into graphite by ball-milling in the presence of red phosphorus was proposed and confirmed by various microscopic and spectroscopic measurements. The resultant GPA was demonstrated to be highly dispersible in various polar solvents, including neutral water for eco-friendly solution processing. Pieces of Hanji coated with solution-cast GPA exhibited very good flame retardation. Hence, the direct introduction of phosphorus into graphite to produce phosphorus-doped GnP using the ball-milling technique and subsequent oxidation into GPA in air moisture could be regarded as a general approach toward low-cost, mass production of GPA for many practical applications, including flame retardation.

METHODS

Preparation of GPA. GPA was prepared by ball-milling the pristine graphite flakes in a planetary ball-mill machine (Pulverisette 6, Fritsch) in the presence of red phosphorus. The pristine graphite (5.0 g, Alfa Aesar, natural graphite, 100 mesh (<150 μm), 99.9995% metals basis, lot# 14735) and red phosphorus (20.0 g) were placed into a stainless steel ball-mill capsule (250 mL) containing stainless steel balls (500.0 g, diameter 5 mm). The capsule was sealed under vacuum. The capsule was fixed in the planetary ball-mill machine and agitated at 500 rpm for 12 and 48 h for GPA12 and GPA48, respectively. The resultant products were Soxhlet extracted with phosphorus tribromide (PBr_3) to completely wash off any residual red phosphorus. Thereafter, 1 M aqueous HCl solution was used to remove metallic impurities, if any, until there was no metallic residue detected by XPS. Final products were freeze-dried at −120 °C under a reduced pressure (0.05 mmHg) for 48 h to yield 8.88 (GPA12, at least 3.88 g $-PO_3H_2$ uptake) and 10.17 g (GPA48, at least 5.17 g $-PO_3H_2$ uptake) of dark black powders, implying the occurrence of the formation of C–P bonds at the edges of GPA.

Preparation of GPA/Hanji and GO/Hanji. Hanji was cut into 10 pieces (3.5 × 7.5 cm). The Hanji specimens were dip-coated in GPA (0.2 mg/mL in water) and GO inks (0.1 mg/mL in water), dried in air for 2 h, and reduced under pressure at 50 °C overnight prior to flame retardation test. In the case of GO/Hanji, multiple coatings were conducted to obtain similar loading level of GO to Hanji.

Conflict of Interest: The authors declare no competing financial interest.

Acknowledgment. This research was supported by Mid-Career Researcher (MCR), BK21 Plus, Basic Science Research (BSR), Basic Research Laboratory (BRL) programs through the

National Research Foundation (NRF) of Korea funded by the Ministry of Education, Science and Technology (MEST), U.S. Air Force Office of Scientific Research through Asian Office of Aerospace R&D (AFOSR-AOARD). L.D. thanks the partial support from AFOSR (FA9550-12-1-0037).

Supporting Information Available: Video of flame retardant test and detailed characterization data from SEM, TEM, XPS, ζ-potential, contact angles, EA, NMR, FT-IR, and Pyro-GC-MS. This material is available free of charge *via* the Internet at http://pubs.acs.org.

REFERENCES AND NOTES

1. Diskowski, H.; Hofmann, T. Phosphorus. In *Ullmann's Encyclopedia of Industrial Chemistry*; Wiley-VCH Verlag GmbH & Co. KGaA: Weinheim, Germany, 2000.
2. Eckstein, F. Nucleoside Phosphorothioates. *Annu. Rev. Biochem.* **1985**, *54*, 367–402.
3. Steck, T. L. The Organization of Proteins in the Human Red Blood Cell Membrane: A Review. *J. Cell. Biol.* **1974**, *62*, 1–19.
4. Bray, R. H.; Kurtz, L. T. Determination of Total, Organic, and Available Forms of Phosphorus in Soils. *Soil Sci.* **1945**, *59*, 39–45.
5. Kennedy, C. S.; Kennedy, G. C. The Equilibrium Boundary between Graphite and Diamond. *J. Geophys. Res.* **1976**, *81*, 2467–2470.
6. Qu, L.; Liu, Y.; Baek, J.-B.; Dai, L. Nitrogen-Doped Graphene as Efficient Metal-Free Electrocatalyst for Oxygen Reduction in Fuel Cells. *ACS Nano* **2010**, *4*, 1321–1326.
7. Dai, L. M. Functionalization of Graphene for Efficient Energy Conversion and Storage. *Acc. Chem. Res.* **2013**, *46*, 31–42.
8. Park, S.; Ruoff, R. S. Chemical Methods for the Production of Graphenes. *Nat. Nanotechnol.* **2009**, *4*, 217–309.
9. Chang, D. W.; Lee, E. K.; Park, E. Y.; Yu, H.; Choi, H.-J.; Jeon, I.-Y.; Sohn, G.-J.; Shin, D.; Park, N.; Oh, J. H.; *et al.* Nitrogen-Doped Graphene Nanoplatelets from Simple Solution Edge-Functionalization for n-Type Field-Effect Transistors. *J. Am. Chem. Soc.* **2013**, *135*, 8981–8988.
10. Jeon, I. Y.; Shin, Y. R.; Sohn, G. J.; Choi, H. J.; Bae, S. Y.; Mahmood, J.; Jung, S. M.; Seo, J. M.; Kim, M. J.; Chang, D. W.; *et al.* Edge-Carboxylated Graphene Nanosheets *via* Ball Milling. *Proc. Natl. Acad. Sci. U.S.A.* **2012**, *109*, 5588–5593.
11. Jeon, I. Y.; Choi, H. J.; Jung, S. M.; Seo, J. M.; Kim, M. J.; Dai, L.; Baek, J. B. Large-Scale Production of Edge-Selectively Functionalized Graphene Nanoplatelets *via* Ball Milling and Their Use as Metal-Free Electrocatalysts for Oxygen Reduction Reaction. *J. Am. Chem. Soc.* **2013**, *135*, 1386–1393.
12. Jeon, I. Y.; Choi, H. J.; Choi, M.; Seo, J. M.; Jung, S. M.; Kim, M. J.; Zhang, S.; Zhang, L.; Xia, Z.; Dai, L.; *et al.* Facile, Scalable Synthesis of Edge-Halogenated Graphene Nanoplatelets as Efficient Metal-Free Eletrocatalysts for Oxygen Reduction Reaction. *Sci. Rep.* **2013**, *3*, 1810.
13. Jeon, I. Y.; Choi, H. J.; Ju, M. J.; Choi, I. T.; Lim, K.; Ko, J.; Kim, H. K.; Kim, J. C.; Lee, J. J.; Shin, D.; *et al.* Direct Nitrogen Fixation at the Edges of Graphene Nanoplatelets as Efficient Electrocatalysts for Energy Conversion. *Sci. Rep.* **2013**, *3*, 2260.
14. Jeon, I.-Y.; Zhang, S.; Zhang, L.; Choi, H.-J.; Seo, J.-M.; Xia, Z.; Dai, L.; Baek, J.-B. Edge-Selectively Sunfurized Graphene Nanoplatelets as Efficient Metal-Free Electrocatalysts for Oxygen Reduction Reaction. *Adv. Mater.* **2013**, *25*, 6138–6145.
15. Seo, J.-M.; Jeon, I.-Y.; Baek, J.-B. Mechanochemically Driven Solid-State Diels–Alder Reaction of Graphite into Graphene Nanoplatelets. *Chem. Sci.* **2013**, *4*, 4273–4277.
16. Chang, D. W.; Choi, H. J.; Jeon, I. Y.; Baek, J. B. Edge-Selectively Functionalized Graphene Nanoplatelets. *Chem. Rec.* **2013**, *13*, 224–238.
17. Clogston, J. D.; Patri, A. K. Zeta Potential Measurement. In *Characterization of Nanoparticles Intended for Drug Delivery*; Springer: Berlin, 2011; pp 63–70.
18. Li, D.; Muller, M. B.; Gilje, S.; Kaner, R. B.; Wallace, G. G. Processable Aqueous Dispersions of Graphene Nanosheets. *Nat. Nanotechnol.* **2008**, *3*, 101–105.
19. Granzow, A. Flame Retardation by Phosphorus-Compounds. *Acc. Chem. Res.* **1978**, *11*, 177–183.
20. Levchik, S. V.; Weil, E. D. A Review of Recent Progress in Phosphorous-Based Flame Retardants. *J. Fire Sci.* **2006**, *24*, 345–364.
21. Zhang, S. A Review of Flame Retardant Polyethylene Fibres. *Prog. Polym. Sci.* **2003**, *28*, 1517–1538.
22. Knox, B. E.; Palmer, H. B. Bond Dissociation Energies in Small Hydrocarbon Molecules. *Chem. Rev.* **1961**, *61*, 247–255.
23. Goldwhite, H. *Introduction to Phosphorous Chemistry*; Cambridge University Press: Cambridge, UK, 1981.
24. Li, Z. Q.; Lu, C. J.; Xia, Z. P.; Zhou, Y.; Luo, Z. X-ray Diffraction Patterns of Graphite and Turbostratic Carbon. *Carbon* **2007**, *45*, 1686–1695.
25. Collins, P. G.; Bradley, K.; Ishigami, M.; Zettl, A. Extreme Oxygen Sensitivity of Electronic Properties of Carbon Nanotubes. *Science* **2000**, *287*, 1801–1804.
26. Bell, R. N. Estimation of Triphosphoric and Pyrophosphoric Acids in Presence of Ortho- and Metaphosphoric Acids. *Anal. Chem.* **1947**, *19*, 97–100.